Школа Поляризованных Нейтронов 2016

Магнитно-электронное фазовое разделение выше T_c в $Sm_{0.32}Pr_{0.18}Sr_{0.5}MnO_3$ манганите.

А.И. Курбаков[1], В.А. Рыжов[1], В.В. Рунов[1], В.В. Дериглазов[1], М.И. Арефьев[1], C. Martin[2], A. Maignan[2]

[1]*Петербургский Институт Ядерной Физики, НИЦ"Курчатовский Институт", Орлова Роща, Гатчина, 188300, Россия*

[2]*Laboratoire CRISMAT, UMR 6508 ISMRA et Universite de Caen, Boulevard de Marechal Juin, 14050 Caen, France*

Mixed-valence manganites

• The doped manganites $La_{1-x}A_xMnO_3$ consist of a 3D network of corner-sharing MnO_6 octahedra located at the nodes of a simple cubic lattice with La(A) in a center of unit cell [M. Pissas et al. Phys. Rev. B **72**, 064425 (2005)].

• The CMR is largest just near the ferromagnetic transition temperature.

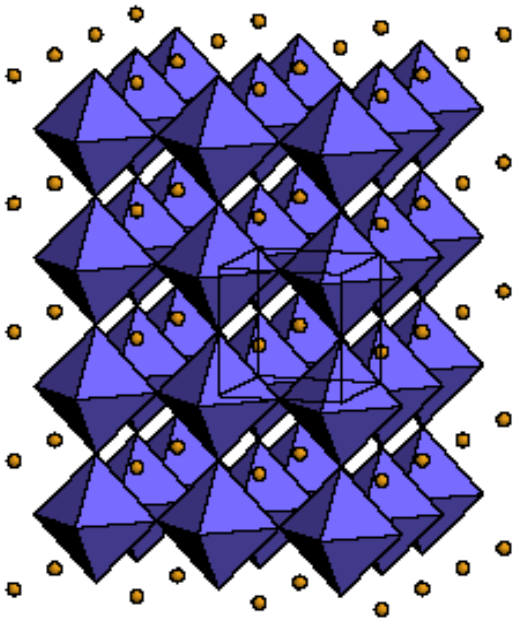

$x\ Mn^{4+} + (1-x)\ Mn^{3+}$

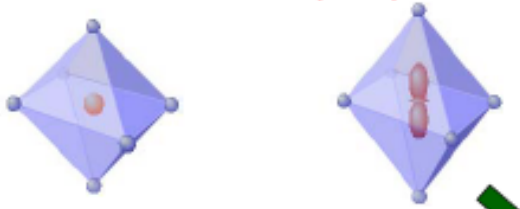

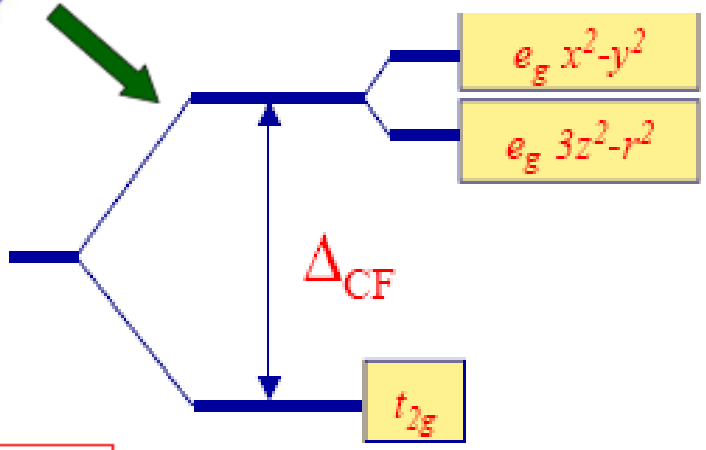

Jahn-Teller provides distortions of MnO_6 octahedra, which effect essentially on structure, probability of e_g-electron hopping as well as create prerequisites for orbital ordering formation.

Jahn-Teller Polarons

Motivation of magneto-electronic phase separation study

Effect of CMR in $Ln_{1-x}A_xMnO_3$ (Ln=La,Pr,Sm; A=Ca,Sr…) perovskite manganites is observed near P-FM transition, both in compounds with insulator (I) and metallic (M) ground states. Magnetic field can change phase equilibrium or temperature of phase transition. The huge change by field of sample resistance R suggests the presence of conductive M phase in it.

Magneto-electronic phase separaton (*MEPS) provides origination of FM-ordered clusters with M properties above T_C embedded in P-I matrix → heterogeneous magnetic state.*

Amount of clusters depends strongly on level of doping, *x*. At approaching their concentration to percolation limit *I-M phase transition* occurs.

So, to insight in physics of manganites one needs to study the details *MEPS and its connection with P-FM, and correlation with structure evolution*

The compounds near half doping are of special interest since they exhibit orbital/charge ordering (OO, CO) followed by AFM ordering that can dramatically effect the MEPS.

Compounds under study

Powdered CMR manganite ***$Sm_{0.32}Pr_{0.18}Sr_{0.5}MnO_3$*** **(*doping $Sm^{3+} \rightarrow Sr^{2+}$ mixed-valence state, large bandwidth W*): main goal of this study is to clarify an effect of isovalent substitution *Sm → Pr* and introduced by it additional disorder on MEPS in comparison with earlier investigated by us ***$Sm_{0.5}Sr_{0.5}MnO_3$*** [PRB 72 (2005) 184432].**

- ***SPSMO:*** **no IMT, MEPS from T*> 307K > T_C~125K; T_{AF-A}~175K; T_{AF-CE}~125K; T_{st}~170K, its structure was studied earlier [Поверхность №6 (2015) 5].**
- ***SSMO:*** **T_{IM} ~ 54K, MEPS from T*> 311K > T_C ~ 110K; T_{AF-A}~135K, T_{st}~ 135K.**
- ***Both crystals exhibit CMR and reveal heterogeneous magnetic state consisting of FM metallic clusters embedded in P matrix, which originates above T_C in a result of MEPS.***

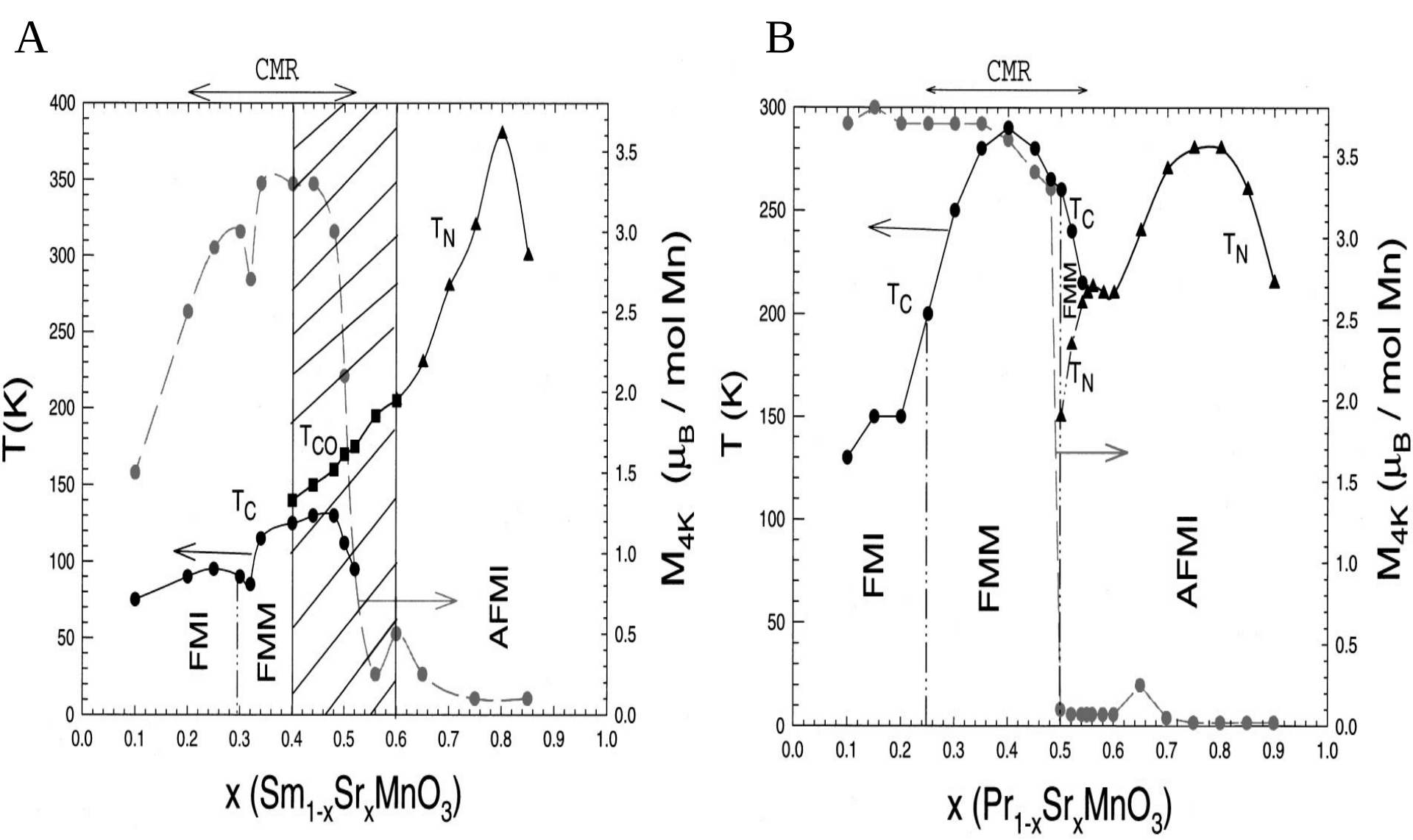

Fig.1. Phase diagrams of $Sm_{1-x}Sr_xMnO_3$: FMM(I), ferromagnetic metal(insulator); CO, charge-ordered insulator; AFMI - antiferromagnetic insulator phase with no long-range JT order. [C. Martin et al. PRB 60 (1999) 12191].

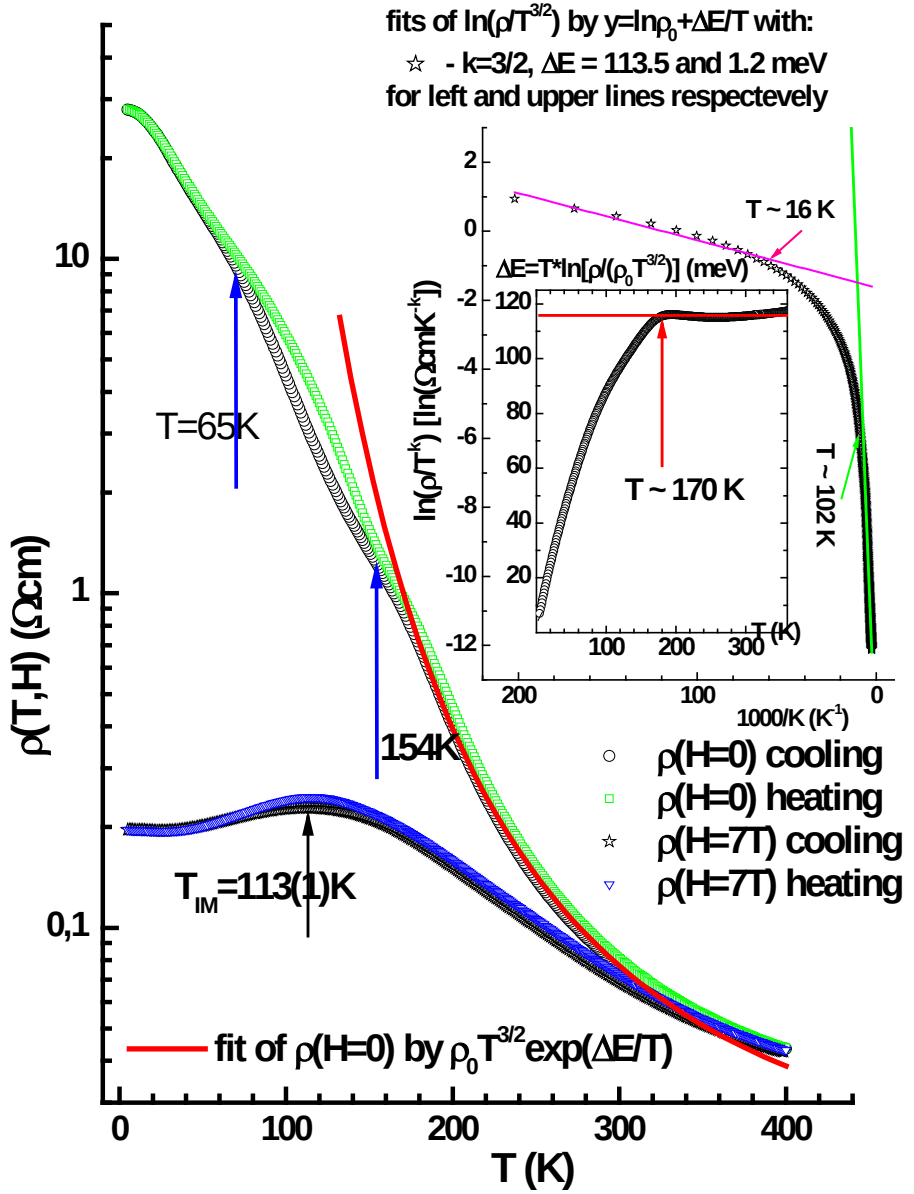

Fig.3. ***T*-dependence of SPSMO resistance at H=0; 7T in direct and reverse T –scan. Red line presents fit of ρ(T) by polaron model. Insert presents ρ in other coordinates.**

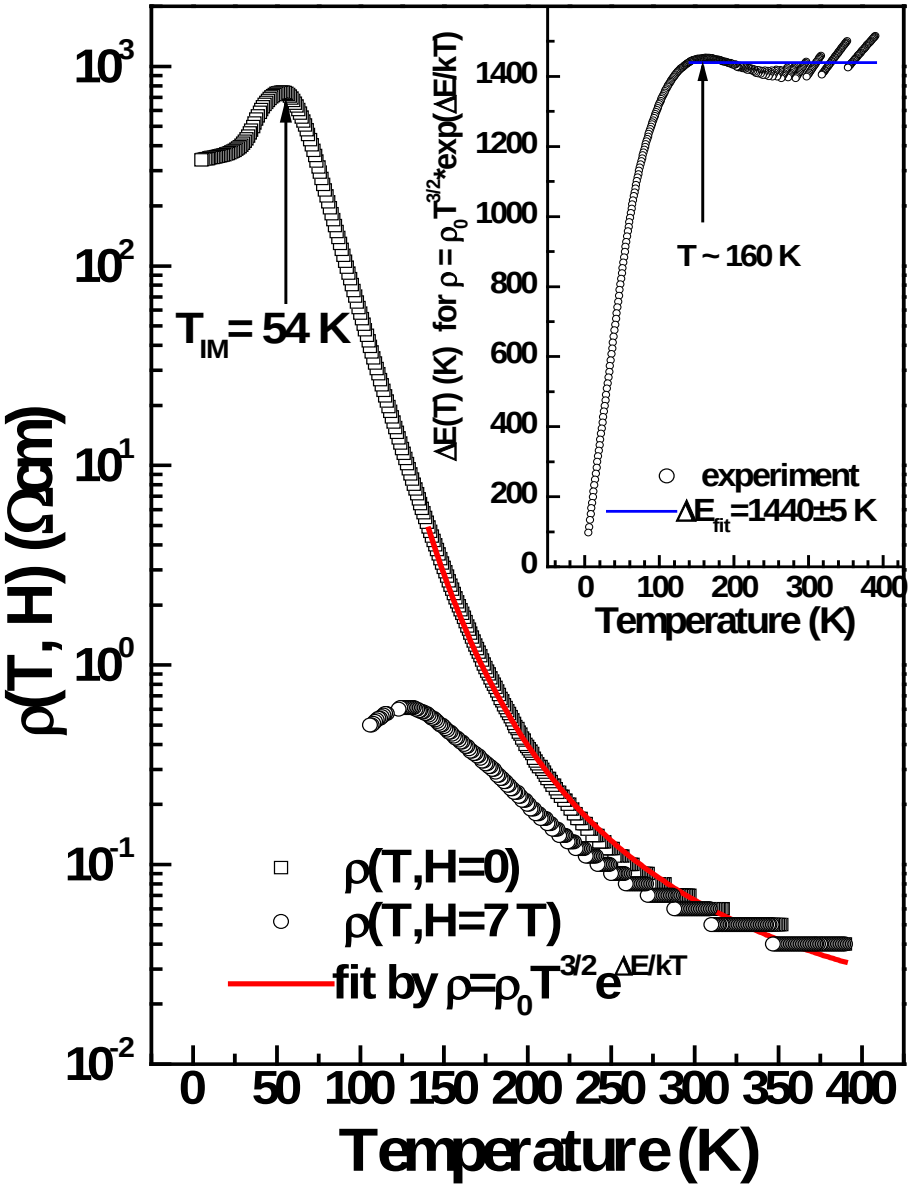

Fig.4.*T*-dependences of SSMO resistance at H = 0; 7 T. Red line presents fit of ρ(T) by polaron model. Insert presents ρ(T) in other coordinates. [Kurbakov et al. PRB **72**, 184432 (2005)]

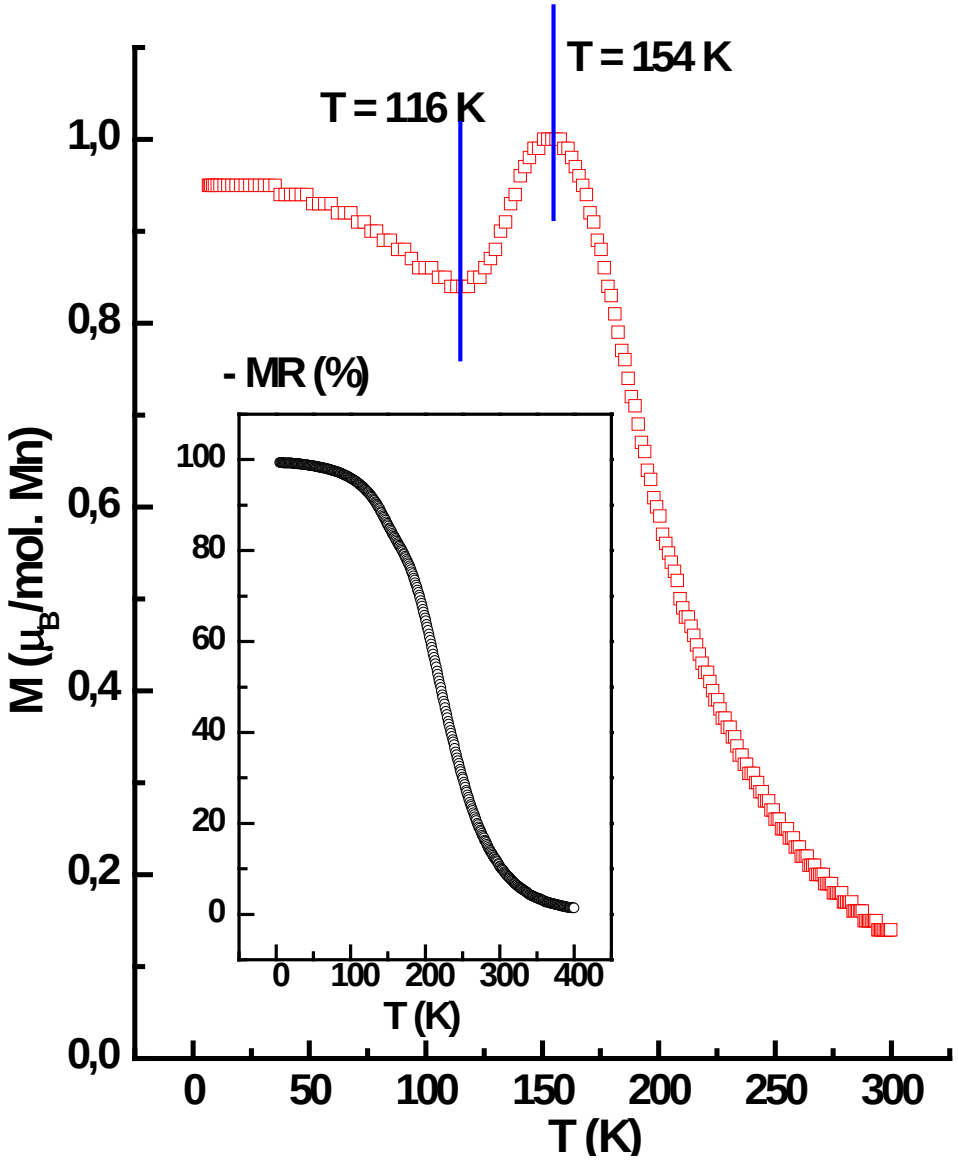

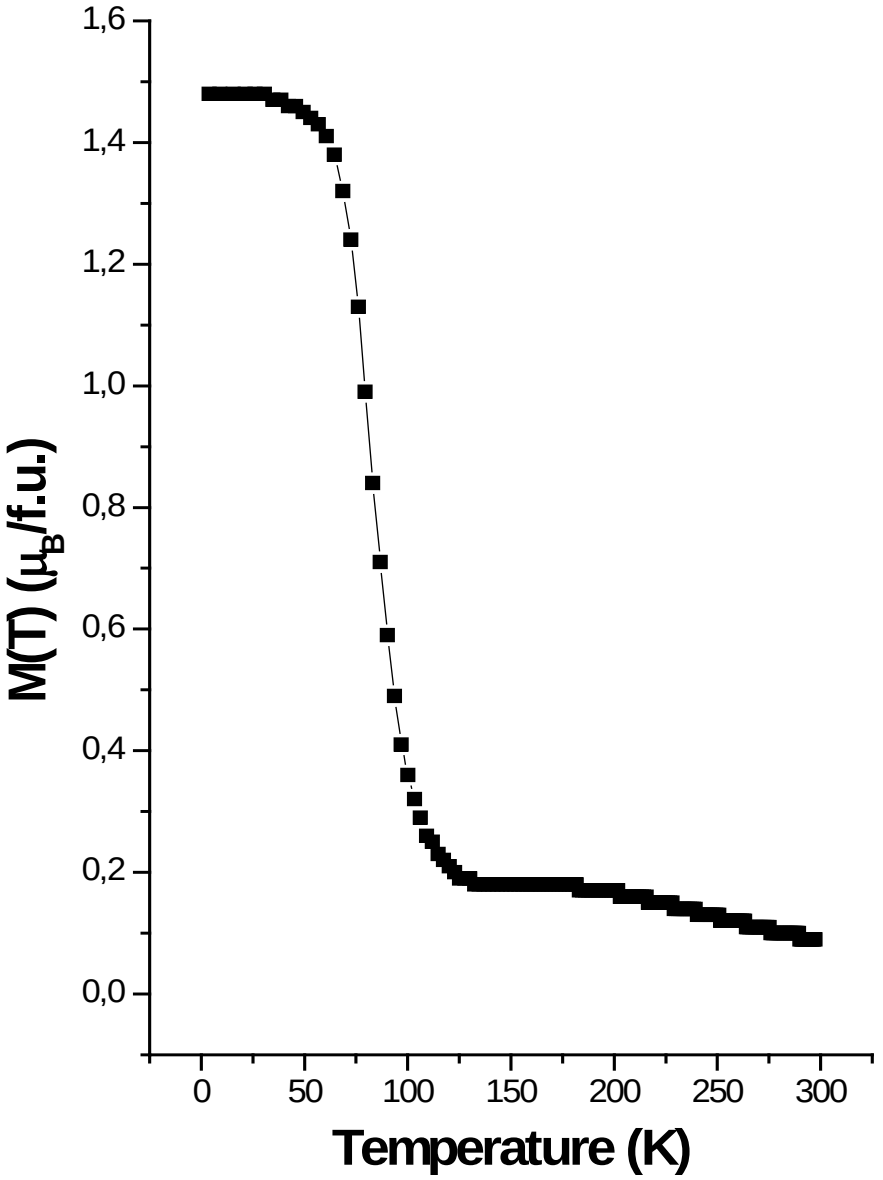

Fig.5.*T*-dependences of M and MR = {[R(H) - R(0)]/R(0)}*100% (insert) in SPSMO.

Fig.6.*T*-dependences of M in SSMO [Kurbakov et al. PRB **72**, 184432 (2005)].

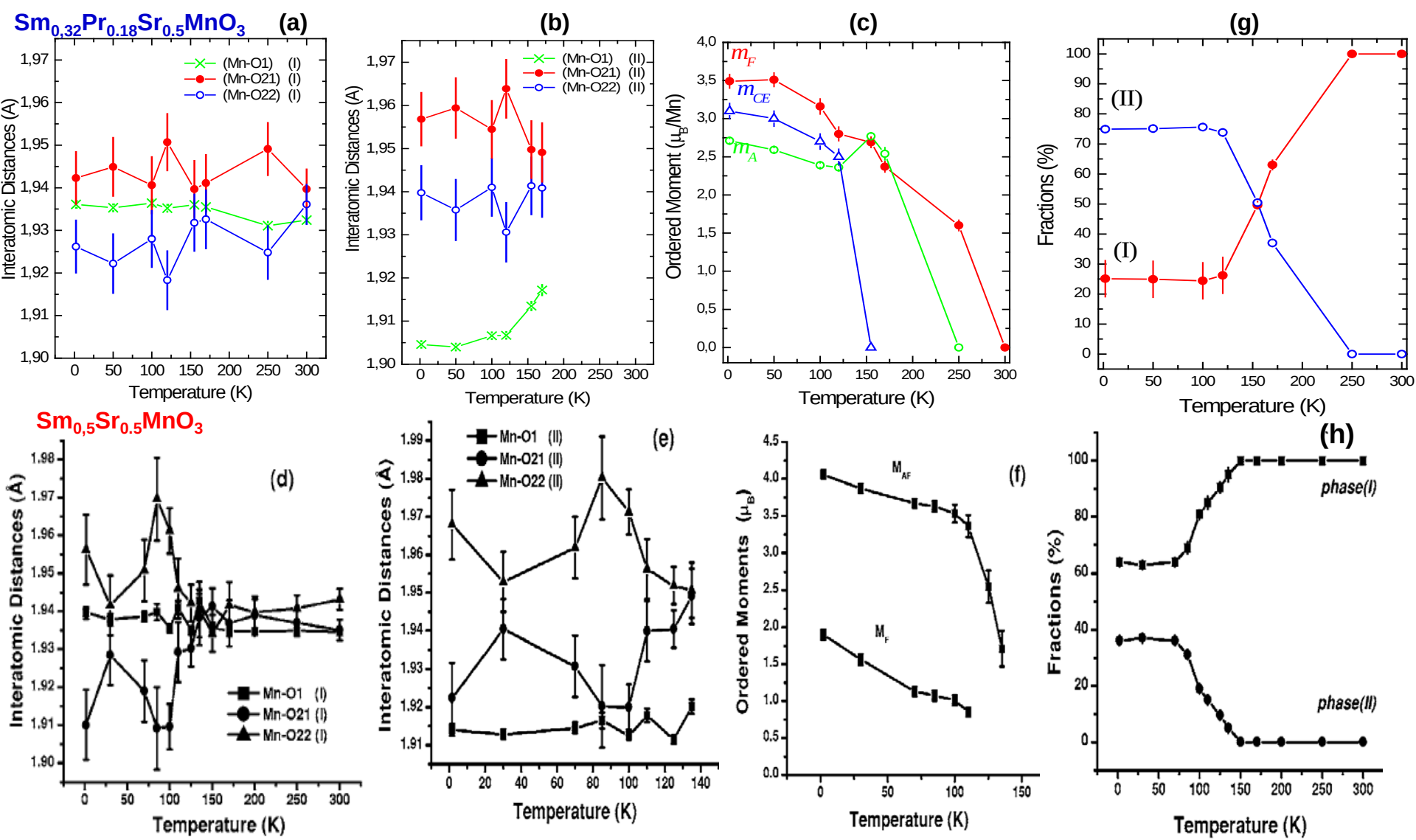

Fig.7. *T*-dependences of interatomic distances (a),(b); (d),(e); moments of different magnetic phases (c), (f); and fractions of structural phases (g), (h) for $Sm_{0.32}Pr_{0.18}Sr_{0.5}MnO_3$ (I –*Pbnm*; II -$P2_1/m$; difference in Mn-O distances for two Mn sites is rather small (deviation of monoclinic angle from 90^0 is small) and we present here average data) and $Sm_{0.5}Sr_{0.5}MnO_3$ (both phases exhibit *Pbnm* space group). In phase I JT distortions are close to that in pure FM $Sm_{0.55}Sr_{0.45}MnO_3$ [Kurbakov et al. Fiz.Tv.Tela 46** (2004) 1650].**

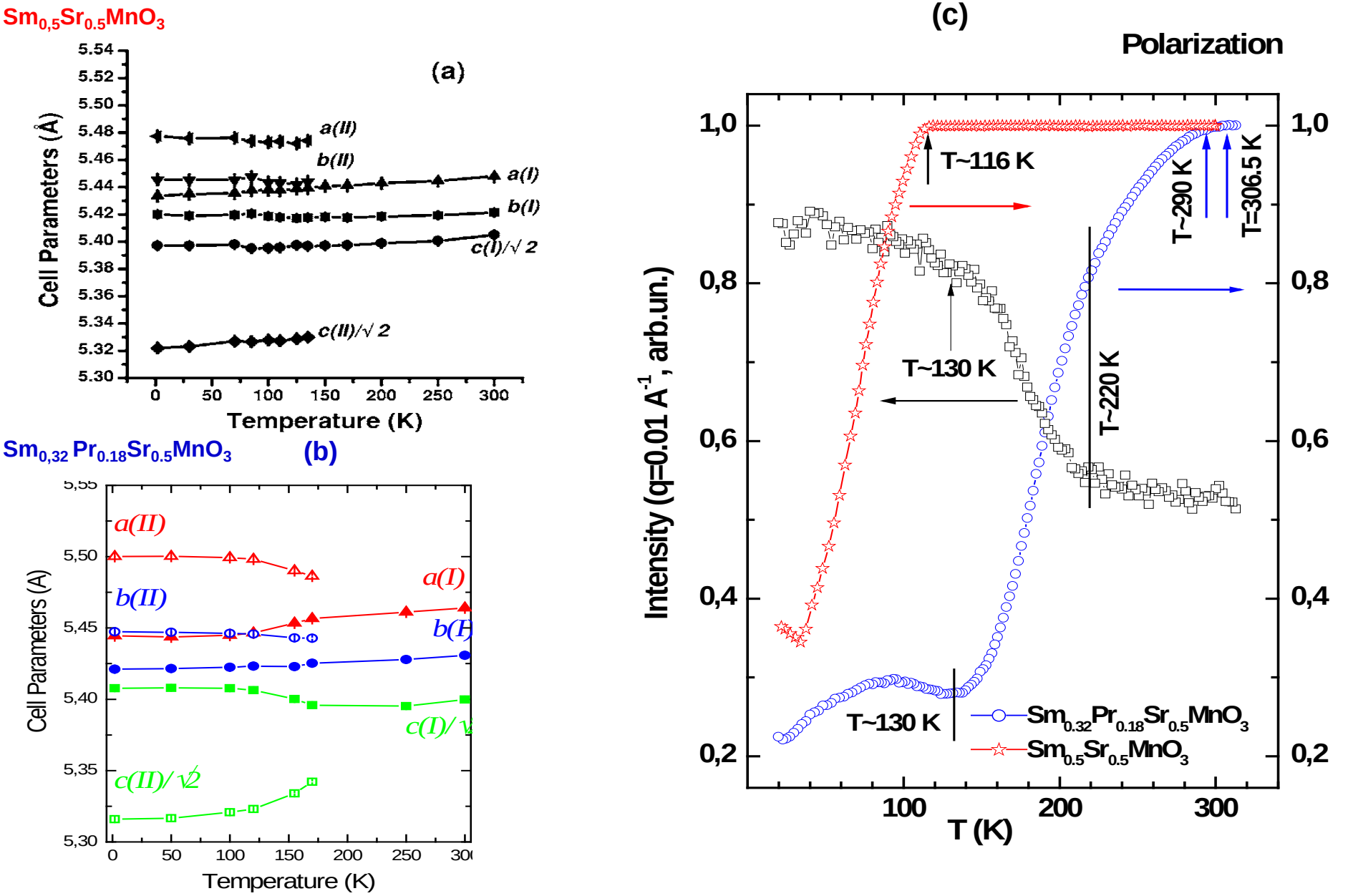

Fig.8. ***T*-dependences of unit cell parameters (a),(b) for $Sm_{0.32}Pr_{0.18}Sr_{0.5}MnO_3$ (I –*Pbnm*; II -$P2_1/m$) and $Sm_{0.5}Sr_{0.5}MnO_3$ (both phases exhibit *Pbnm* space group). Panel (c) presents the data on *polarization* for both samples and *small angle polarized neutrons scattering* (SAPNS) for the former.**

Second harmonic of magnetization, M_2 of nonlinear response in longitudinal geometry: parallel steady and ac - harmonic magnetic fields ($H(t) = H + h\cos\omega t$)

- When $M_2 \propto h^2$, $M_2(\omega,H) = \chi_2(\omega,H)\, h^2$, χ_2 – susceptibility of second order with static limit
- $\chi_2(0,H) = \mathrm{Re}\chi_2(0,H) = (1/2)\partial^2 M(H)/\partial H^2$, $\mathrm{Im}\chi_2(0,H)=0$. In isotropic case from Blox eq.

$$\chi_2(\omega) = \Gamma(-i2\omega+\Gamma)^{-1}\chi_2(0) - i\omega(\partial\Gamma/\partial H)\{(-i2\omega+\Gamma)(-i\omega+\Gamma)\}^{-1}\chi_1(0). \quad (1)$$

The first term in $\chi_2(\omega)$ is due to nonlinearity of $M(H)$. It gives main contribution to $\mathrm{Re}M_2$.

Second term is owing to effect of external magnetic field on relaxation processes. It gives main contribution to $\mathrm{Im}M_2$ and its sign is opposite to that of $\mathrm{Re}M_2$.

- M_2 - pseudovector and even function of $h \Rightarrow M_2(H)$ - odd in H with $M_2(0) = 0$ in paramagnetic ph ase ($M_2 \propto H$ at $H \to 0$).

High sensitivity to appearance of spontaneous magnetization, since in this case $M_2 \neq 0$ at $H = 0$.

Expectations for M_2 in 3D isotropic ferromagnet above T_C

$\omega/\Gamma << 1$ ($\Gamma > 500$ Oe (ESR)) $\Rightarrow \mathrm{Re}M_2(\omega,H) \propto \mathrm{Re}\chi_2(0) \propto \partial^2 M(H)/\partial H^2$. In weak field regime ($g\mu H < \Omega(\tau) = kT_C\tau^{5/3}$), $\mathrm{Re}M_2 \propto H\tau^{-14/3}$ (crossover to strong field regime at $\tau_H = (g\mu H/kT_C)^{3/5} = 2.2\cdot10^{-4}$ {$H = 300$ Oe, $T_C \sim 186$ K}, $T_H \sim T_C + 0.1$ K.

$\mathrm{Im}M_2$ has more complicated behavior (approximately linear in H) being related to a spin diffusion mode. In the first approximation $\mathrm{Im}M_2 \propto H\tau^{-19/6}$. **Thus:**

$\mathrm{Re}M_2 \propto H\tau^{-14/3}$; $\mathrm{Im}M_2 \propto H\tau^{-19/6}\cdot G(H,\tau)$, G is known, weakly changed function.

Expectations for M_2 of ensemble of non-intaracting FM clusters possessing by large magnetic moment

They should exhibit large nonlinearity of $M(H)$ in a weak H ***due to their large moment.*** **This** will provide M_2 **signal with extremum in weak field.** Above T_C, the latter can be easily distinguished from linear on H response of matrix.

The regime of magnetic behavior of FM clusters (superparamagnetic (SPM)/ hysteretic with dynamic H-hysteresis) will depend on relation of cluster anisotropy energy ($E_{an} = Kv$, K - effective anisotropy constant, v - average volume of clusters) and thermal fluctuations.

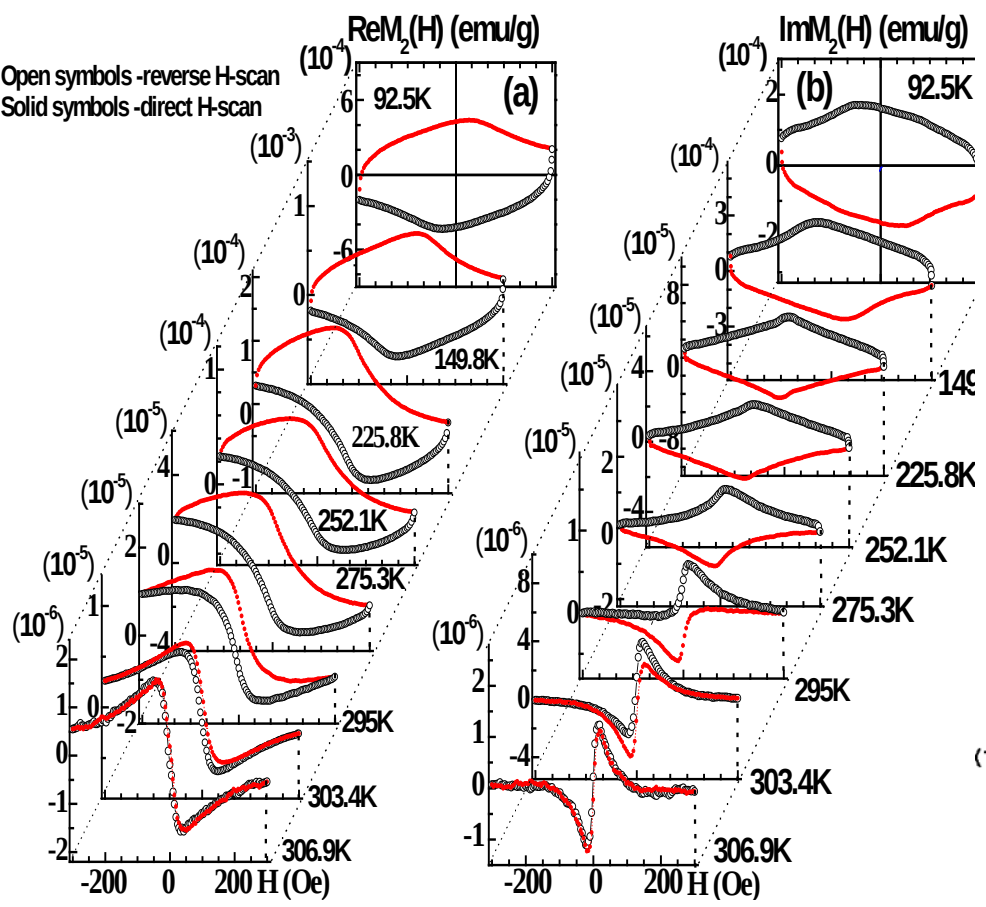

(a) $Sm_{0.32}Pr_{0.15}Sr_{0.5}MnO_3$

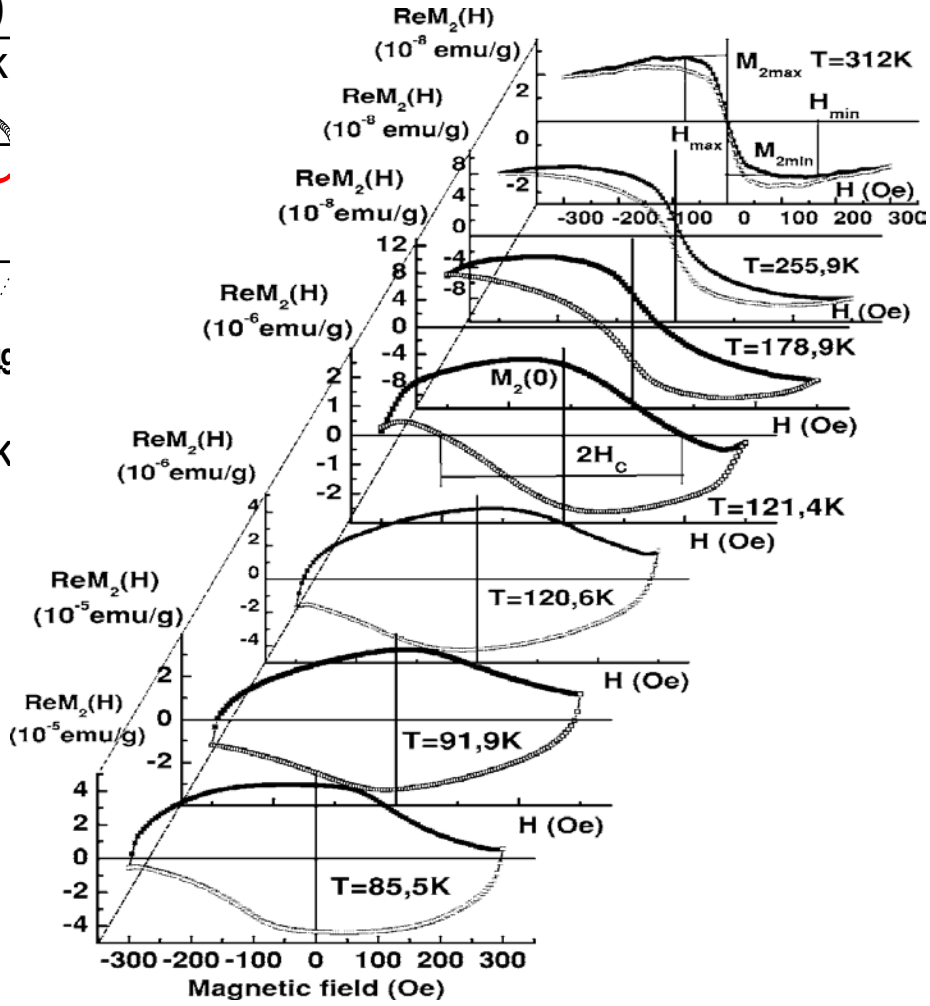

(b) $Sm_{0.5}Sr_{0.5}MnO_3$

Fig.9. Phase components of second harmonic of magnetization, M_2, of NLR as functions of the steady field H at some T: (1) for SPSMO (T^*> 307K > T_C ~ 125K; T_{coal} ~ 270 K) - panel (a); (2) for SSMO (T^*~ 312K > T_C ~ 110K > T_{IM} ~ 54K; T_{coal} ~ 120 K) – panel (b). Concentrations of clusters become close at temperatures of depolarization beginning. **M_2 signal from cluster subsystem in critical region of matrix P-FM transition is too large and masks matrix signal.**

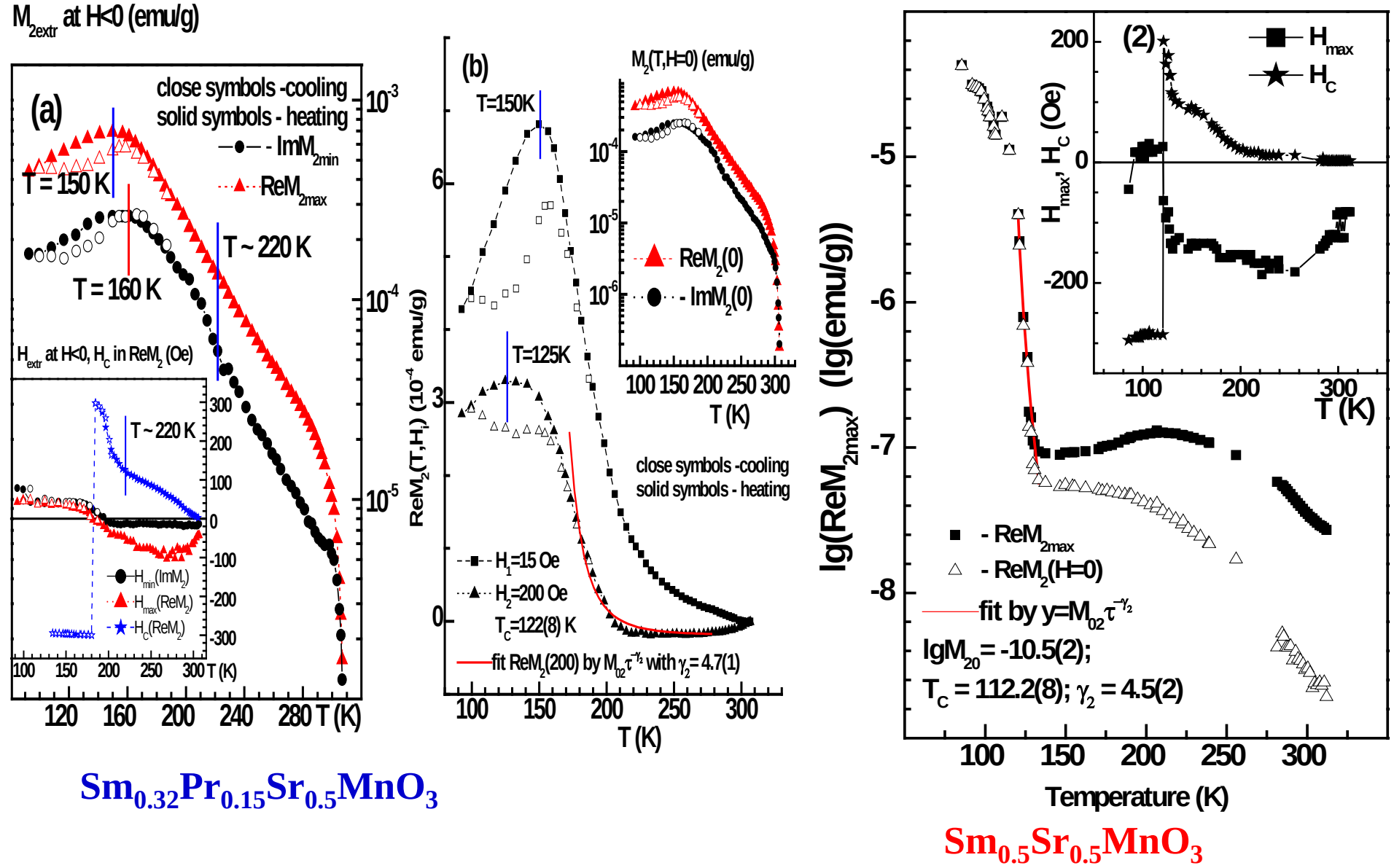

$Sm_{0.32}Pr_{0.15}Sr_{0.5}MnO_3$

$Sm_{0.5}Sr_{0.5}MnO_3$

Fig.10. *T*-dependences of M_2-response parameters for SPSMO (left panel) and SSMO (right panel) compounds. For first sample Panel (a) shows values of M_2 in extremes, M_{ext}; insert in (a) presents positions of extreme, H_{ext}, and "coercive force" H_C; Panel (b) shows cross-sections of Re$M_2(H,T)$ at H =15; 200 Oe, fit of the latter by scaling law; inset displays value of Re(Im)M_2 at H=0. For SSMO, right panel presents ReM_2 value in extreme, its fit and Re$M_2(H=0)$ characterizing H-hysteresis; in shows positions of extreme, H_{max} and "coercive force" H_C in ReM_2.

Description of SPM clusters magnetic dynamics is based on Gilbert stochastic equation (it is analog of Lanzheven diffused equation) [J. L. Garcia-Palacios, Adv. Chem. Phys. **112, 1 (2007)**]:

$$\frac{\mathbf{dm}}{\mathbf{dt}} = \gamma \mathbf{m} \times \left[\mathbf{B}_{eff}(t) + \mathbf{b}_{fl}(t) - (\gamma m)^{-1} \alpha \frac{\mathbf{dm}}{\mathbf{dt}} \right]$$

Here **m** –cluster magnetic moment, $\mathbf{B_{eff}} = \partial V / \partial \mathbf{m}$ is effective magnetic field, $V(t)$ –magnetic potential, $\mathbf{b}_{fl}$ is a weak fluctuating magnetic field.

Kinetics of FM cluster ensemble is obeyed to Fokker-Planck equation [S.V. Titov et al. PRB **82, 100413(R) (2010)]:**

$$2\tau_N \frac{\partial W}{\partial t} = \frac{\beta}{\alpha} \mathbf{u} \cdot (\nabla V \times \nabla W) + \nabla(\nabla V + \beta W \nabla V) \qquad \textbf{(3)}$$

The first term in right part of (3) describes a precession. The second term describes a rotational diffusion of unit vector $\mathbf{u} = \mathbf{M}_s/M$ of magnetization $\mathbf{M}_s$ and is responsible for thermal relaxation.

Here W – nonequilibrium distribution function of probability density for directions $\mathbf{u} = \mathbf{M}_s/M$; $\nabla = \partial/\partial\mathbf{u}$ – gradient operator; $\beta = v/k_BT$, where v – cluster volume, k_B - Boltzmann constant, T – temperature. diffusion relaxation time is taken in form of Landau-Lifshitz $\tau_N = \tau_0/\alpha$, where α – damping factor and $\tau_0 = \beta M_s/2\gamma$ (γ – gyromagnetic ratio).

τ_N is the characteristic time of diffusion in absense of potential.

Magnetic potential V is usually implied uniaxial [H. El Mrabti et al. J. Appl. Phys. **110, 023901 (2011)**]:

$$\beta V = \sigma \sin^2 \vartheta - \xi_H \mathbf{u} \cdot \frac{\mathbf{H}}{H} - \xi_h \mathbf{u} \cdot \frac{\mathbf{h}}{h} \cos \omega t, \qquad \textbf{(4)}$$

Here $\xi_H = \beta M_s H$ and $\xi_h = \beta M_s h$; **H** and **h** – steady and AC magnetic fields accordingly. The first term in(4) – anisotropy energy with $\sigma = \beta K_a$, where $\beta = v/k_BT$, K_a – effective constant of anisotropy, including magneto-crystal anisotropy, form anisotropy and surface one; ϑ - angle between anisotropy axis and magnetization, second and third terms – Zeeman energy.

Decision for distribution function:

$$W(t, \vartheta, \varphi) = \sum_{l=0}^{\infty} \sum_{m=-l}^{l} c_{lm}(t) Y_{lm}(\vartheta, \varphi)$$

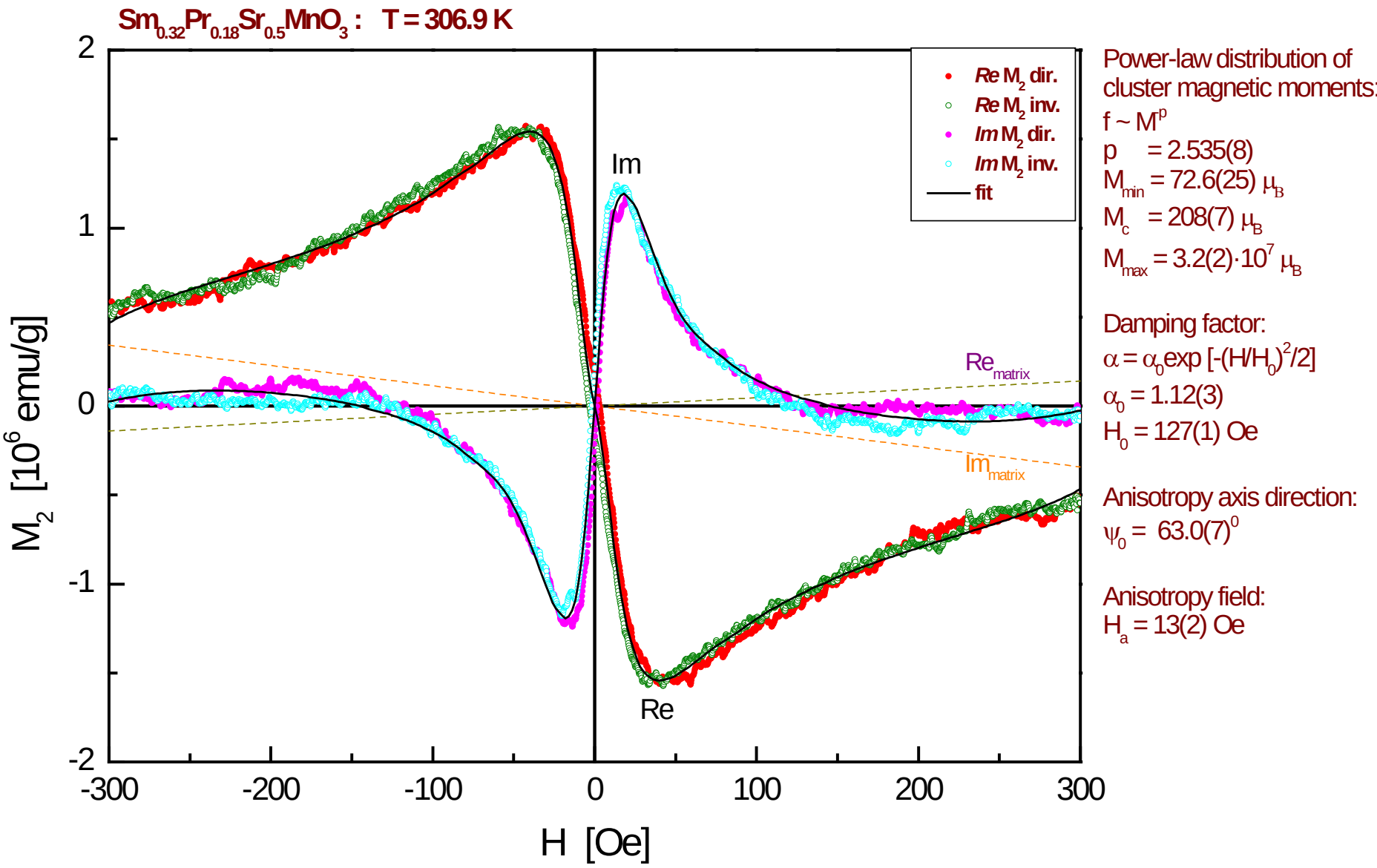

Fig.11. Fit of SPSMO compound M_2-response by decision of Fokker-Plank equation. T = 306.9K. Power-law distribution of clusters was used. Since a presence of a weak H-hysteresis **the curves (Re(Im)M_{2dir}+ Re(Im)M_{2rev})/2 were fitted. The dynamical parameters can be found by this approach only.**

Peter the Great SPb Polytechnic University cluster was used in these calculations.

Заключение

I. Нейтронная дифракция показывает сходную эволюцию структуры в SSMO и SPSMO образцах: присутствует структурный переход из орторомбической псевдокубической фазы с небольшими ЯТ искажениями I в низкотемпературную фазу II с существенно большими искажениями и орбитальным порядком (орторомбическую и моноклинную соответственно). Дальний ФМ порядок образуется только в фазе I. Фаза II испытывает АФ упорядочение А-типа в SSMO и комбинацию А- и псевдо CE-типов упорядочения в SPSMO образце. Отметим, что похожий сценарий эволюции структуры наблюдался и в $Pr_{0.5}Sr_{0.5}MnO_3$ манганите [Damay et al. JMMM 184 (1998) 71].

II. Оба образца обладают свойством КМС, при этом SSMO испытывает И-М переход, а SPSMO – нет. Данные по M(T) определенно указывают на присутствие АФ упорядочения во 2-м образце.

III. Зависимость поляризации от T разительно отличается: в то время как в SSMO деполяризация лишь в области ниже 120 K, в SPSMO она стартует с 307 K. Измерения SAPNS ($q = 0.01$ Å^{-1}) позволили отследить развитие структурного перехода в SPSMO.

IV. Измерения M_2 показали, что образование кластеров , обладающих ФМ компонентой начина-ется выше комнатной температуры ($T^* > 310$ K). Однако в SSMO их концентрация растет очень слабо, показывая широкий максимум и затем уменьшение, и остается ~ на 2 порядка ниже, чем в SPSMO вплоть до $T \sim 120$ K < T_C, *ниже которой начинается деполяризация.* В то же время в SPSMO деполяризация начинается практически сразу ниже 320 K, а концентрация кластеров быстро растет и сопровождается их коалесценцией. Это приводит, по-видимому, к перколяцион-ному И-М переходу в отдельных кристаллитах образца с фазой I, сопровождающемуся образованием дальнего ФМ порядка перколяционного типа, который проявляется в ND при $T \sim 270$ K. Это подтверждает отсутствие И-М перехода во всем образце, предположительно за счет малого количества этой фазы (< 20%). КМС наблюдается, по-видимому, за счет метамагнитного перехода («плавления» АФ фазы) под действием поля в кристаллитах с фазой II. Необычное поведение кластеров в SSMO можно объяснить АФ характером (с присутствием заметной ФМ компоненты) их упорядочения.

Вносимый изовалентным замещением слабый дополнительный беспорядок, по-видимому, способствует образованию ФМ кластеров.

V. Использование кинетического уравнения Фоккера-Планка для анализа M_2 отклика в области его безгистерезисного поведения (суперпарамагнитный режим поведения кластеров) с использованием данных деполяризации нейтронов позволяет, в принципе, определить геометрические и динамические параметры кластеров. В случае SPSMO состава анализ указывает на степенную функцию распределения размеров класте-ров с показателем 2.55 (фрактальная размерность кластеров), что нуждается в дальнейшей проверке.

THE END

Thank you for your attention

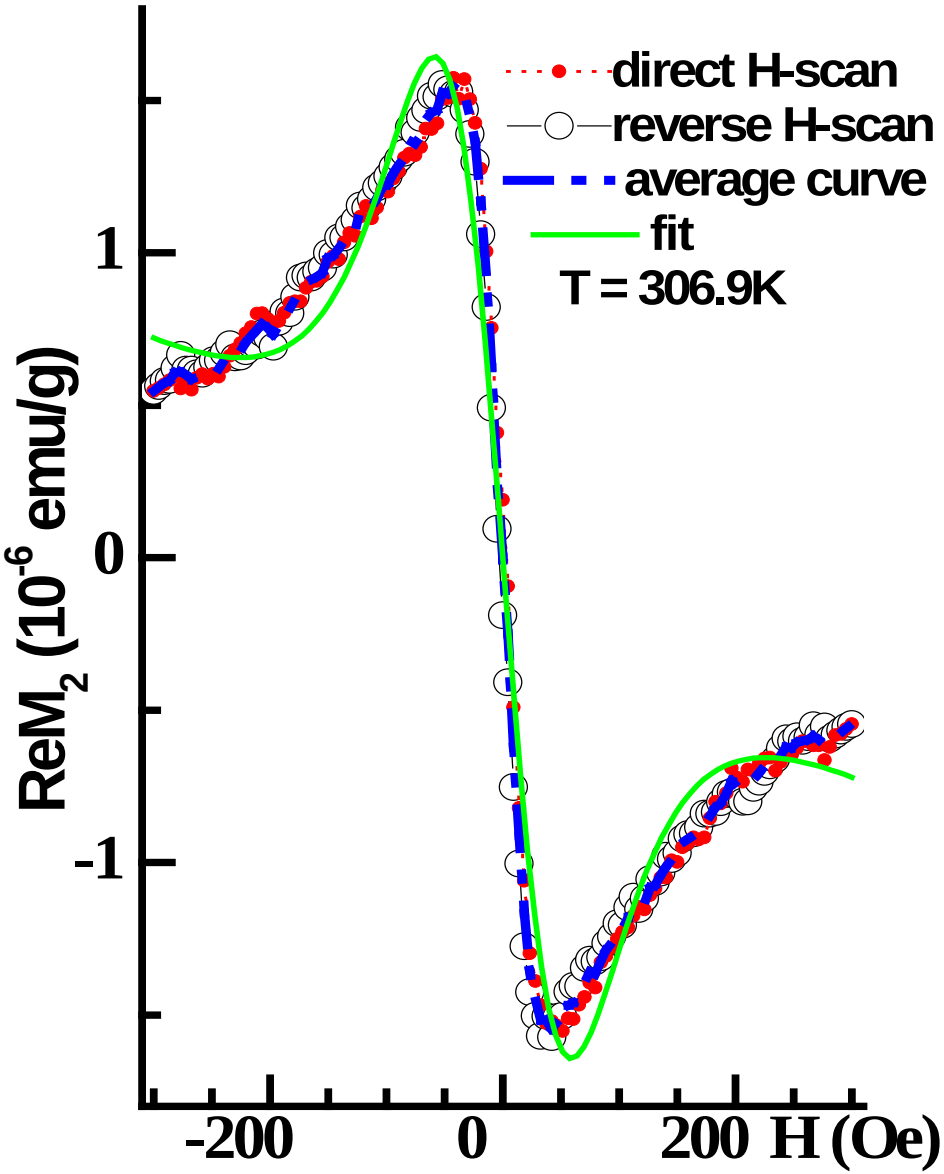

Fig.12. Fit of SPSMP compound ReM_2-response by Eq. 1 in static limit with M described Lanzheven function + linear on H response of matrix. T = 306.9K. $\mu \sim 1.1 \cdot 10^5\ \mu_B$, $N_{cl} \sim 1.5 \cdot 10^{14}$ 1/g.

Full Hamiltonian

$$H = H_{\text{kin}} + H_{\text{Hund}} + H_{\text{AFM}} + H_{\text{el-ph}} + H_{\text{el-el}};$$

there are five important ingredients that regulate the physics of electrons in manganites:

(i) H_{kin} **- the kinetic term of the** e_g **-electrons.**

(ii) H_{Hund} **- the Hund coupling between the** e_g**-electron spin and the localized** t_{2g}**-spin.**

(iii) H_{AFM} **- the AFM Heisenberg coupling between nearest-neighbor** t_{2g} **-spins.**

(iv) $H_{\text{el-ph}}$ **- the coupling between the** e_g**-electrons and the local distortions of the** MnO_6 **octahedron.**

(v) Hel-el - **the Coulomb interactions among the eg-elec**t_r**ons (□0.7 eV).**

This expression is believed to define an appropriate starting model for manganites, but, unfortunately, it is quite difficult to solve such a Hamiltonian of manganites, and some simplifications are usually used.

One-or*bital double-exchange model (Zener***, 1951; Furukawa, 1994)**

$$\mathrm{H}_{\mathrm{DE}} = -t \sum_{<i,j>,\sigma} (a^{T*}_{i\sigma} a_{j\sigma} + h.c.) - J_H \sum_i s_i S_j + J_{AF} \sum_{<i,j>} S_i S_j$$

t □0.*3 e***V; JH □1** e_V**; JAF □0.**$_{01}$ **eV;**

where ai□is t_{he} **annihilation operator for an electron with spin □at site i, but** ***w*****ithout orbital index. Note that HDE is** q_{ua}**dratic in the electron operators, indicating that it is reduced to a one-electron problem eg spin** $_s$**i = □□/□***q*†*i*$\gamma_{\alpha\sigma\alpha}$□$_{ai\gamma}$$\beta_o$***n*** $_{the}$ **background of localized t2g spin**n_s **S.**

In absence of external magnetic field cluster moments are oriented along anisotropy axis, the moment of ensemble being **M** = 0. To reach thermal equilibrium at field turning on, magnetic moments of part of ensemble should change their orientation on angle *π.* The latter is required the transition across barrier (Fig.7) under action of thermal fluctuation. **The relaxation time is described by Neel-Brown expression:**

$$\tau = \tau_0 \exp(\Delta E_B / kT), \qquad \Delta E_B = K_a v \qquad (3)$$

Here K_a is effective anisotropy constant, v – cluster volume, $\tau_0 \sim 10^{-10}$ s. Transition from superparamagnetic regime to blocking one, which is characterized by H-hysteresis arising in M(H) и *M2*(H) is determined by condition: $\tau_{meas} \approx \tau$, from which the blocking temperature can be found:

$$T_B \approx K_a v / [k \cdot \ln(\tau_{meas}/\tau_0)] \qquad (4)$$

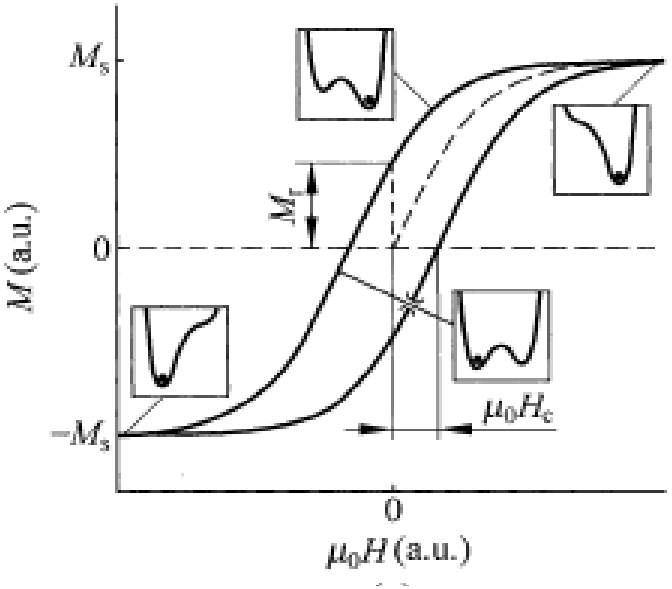

Fig.8. Magnetic hysteresis: (a) origin and phenomenology of hysteresis. The insets are energy-landscape equivalents of the magnetization

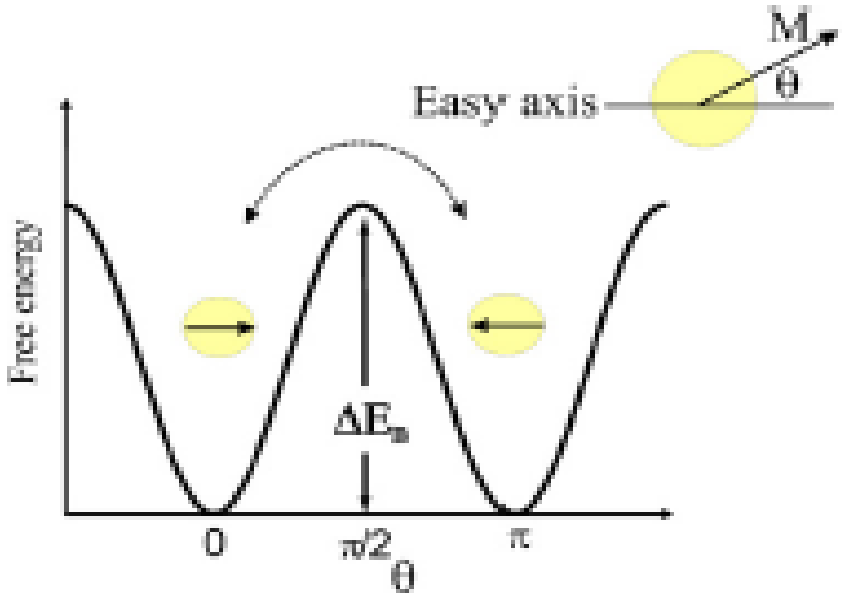

Fig. 7. Schematic picture of the free energy of a single-domain particle with uniaxial anisotropy as a function of magnetization direction. ΔE_B *is the energy barrier hindering the free rotation of the* magnetization and *θ is the angle between the magnetization M and* the easy axis. [S. Bedanta and W. Kleemann. J.Phys.D: App,Phys. **42** (2009) 013001].

Inserts in **Fig. 8** show schematically a change of barrier for FM clusters in two-well potential in presence of external magnetic field:

$$\Delta E_B = K_a v + \mu H(t). \qquad (5)$$

Thus, relaxation time (3) will be function of external field, and in $M_2(H,T)$ *will appear high harmonics provided by this parametrics.*

From expression (4) is clear the dependence of blocking temperature T_B on cluster dimension, and *H*-hysteresis of $M_2(H)$ response on frequency of *H*-scan, F_{sc}, of steady field *H.* **For the latter,** in case of signal accumulation at periodic *H*-scan the time of measurement is $\tau_{meas} = 1/F_{sc}$.

Электронная структура ионов Mn

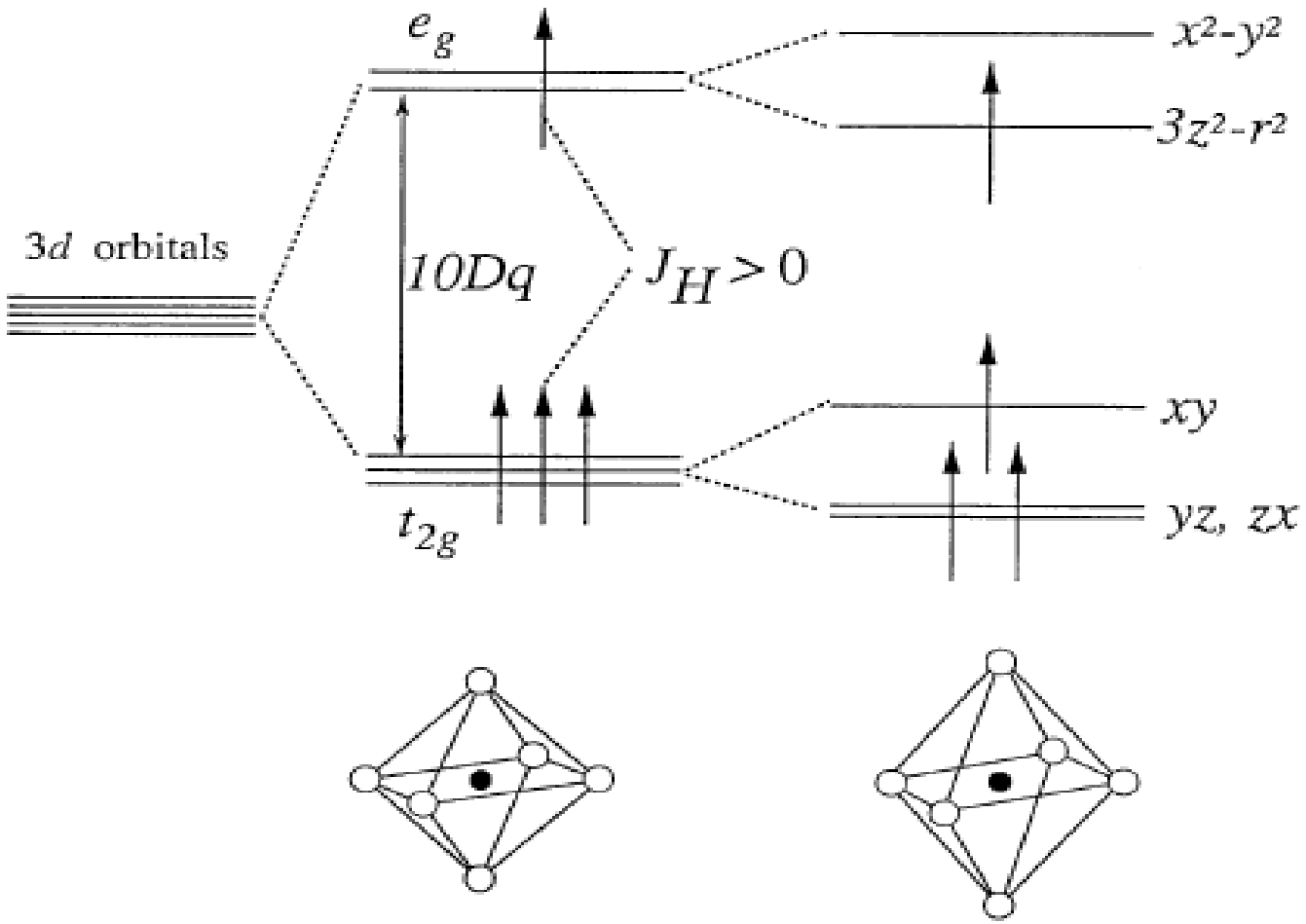

Field splitting of the five-fold degenerate atomic 3*d* levels into lower *t* and higher *e* levels. The particular Jahn-Teller distortion sketched in the figure further lifts each degeneracy as shown. $J_{CF} \sim 2$ eV, $J_H \sim 2 - 3$ eV, $J_{JT} \sim 0.5$ eV, t ~0.3 eV.

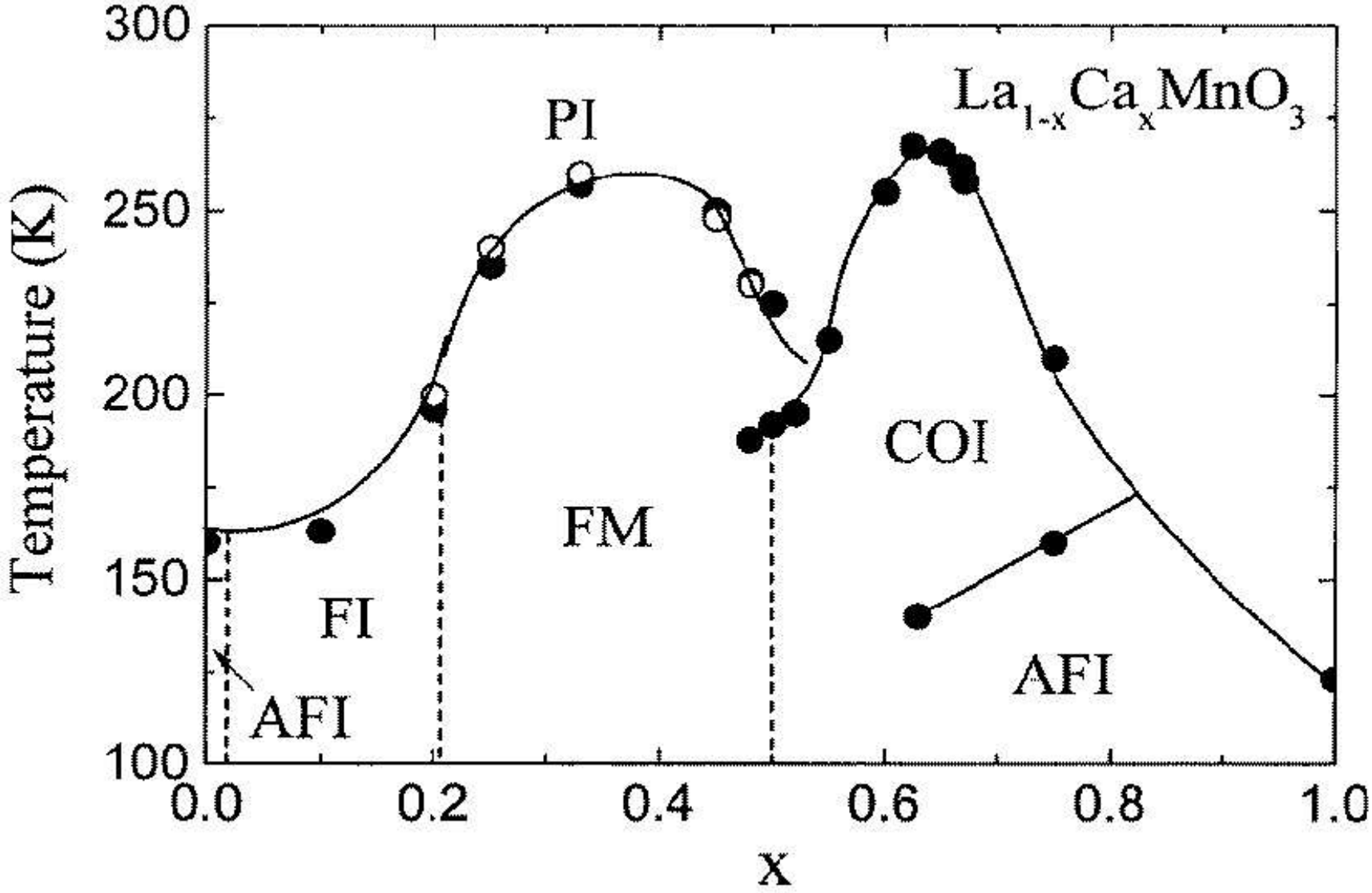

Magnetic and electronic phase diagram versus doping *x* for $La_{1-x}Ca_xMnO_3$ (medium band width). [Schiffer P., Ramirez A. P., Bao W. and Cheong S-W. *Phys. Rev. Lett.* ***75,*** 3336 (1995)]

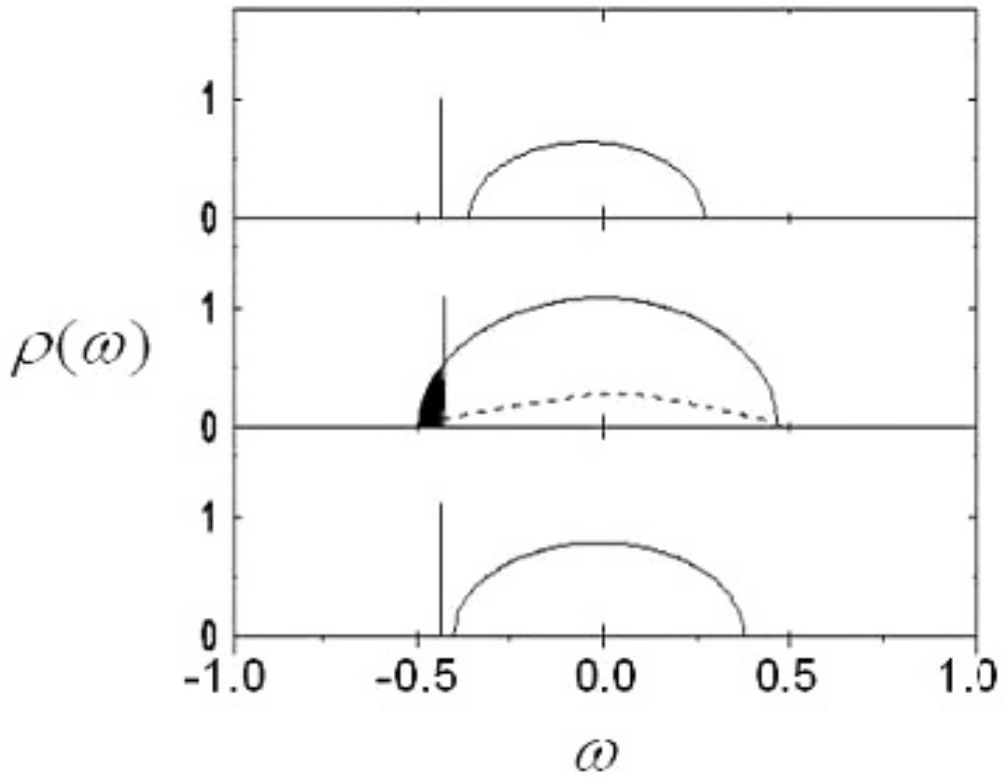

Two band model.

Spectral density (E_{JT} = - 0.5 eV, D = 1.2 eV, U = 5 eV, J_F = 2 meV) : (a) x = 0.1, T = 0 (FI), (b) x = 0.3, T = 180 K (< T_C =240 K) (FM), occupied band states are shown shaded, (c) T = 350 K (PI). Vertical line is the *l* polaron level.

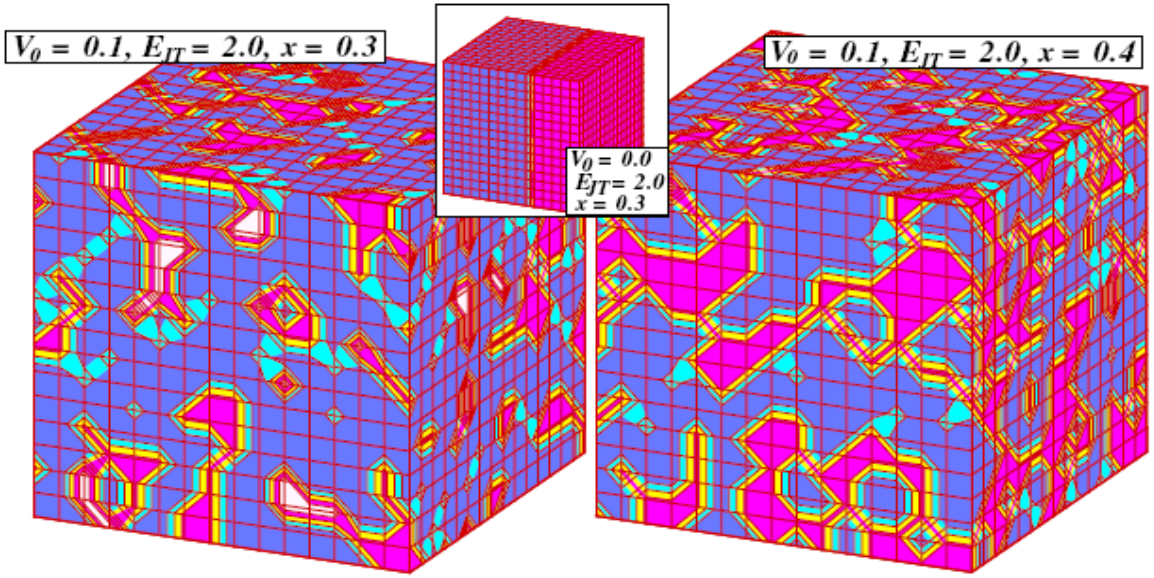

FIG. 1 (color online). Real space electronic distribution obtained from simulations on a 16^3 cube. Magenta (darkest) denotes hole clumps with occupied b electrons, white (lightest) denotes hole clumps with no b electrons, cyan (2nd lightest) denote singleton holes, and light blue (2nd darkest) represents regions with ℓ polarons. Left: Isolated clumps with occupied b electrons (b-electron puddles). Right: Larger doping; percolating clumps. Inset: ''macroscopic phase separation'' absence of long range Coulomb interaction ($V_0 = 0.0$).

V.B. Shenoy et al., PRL 98, 066602 (2007)

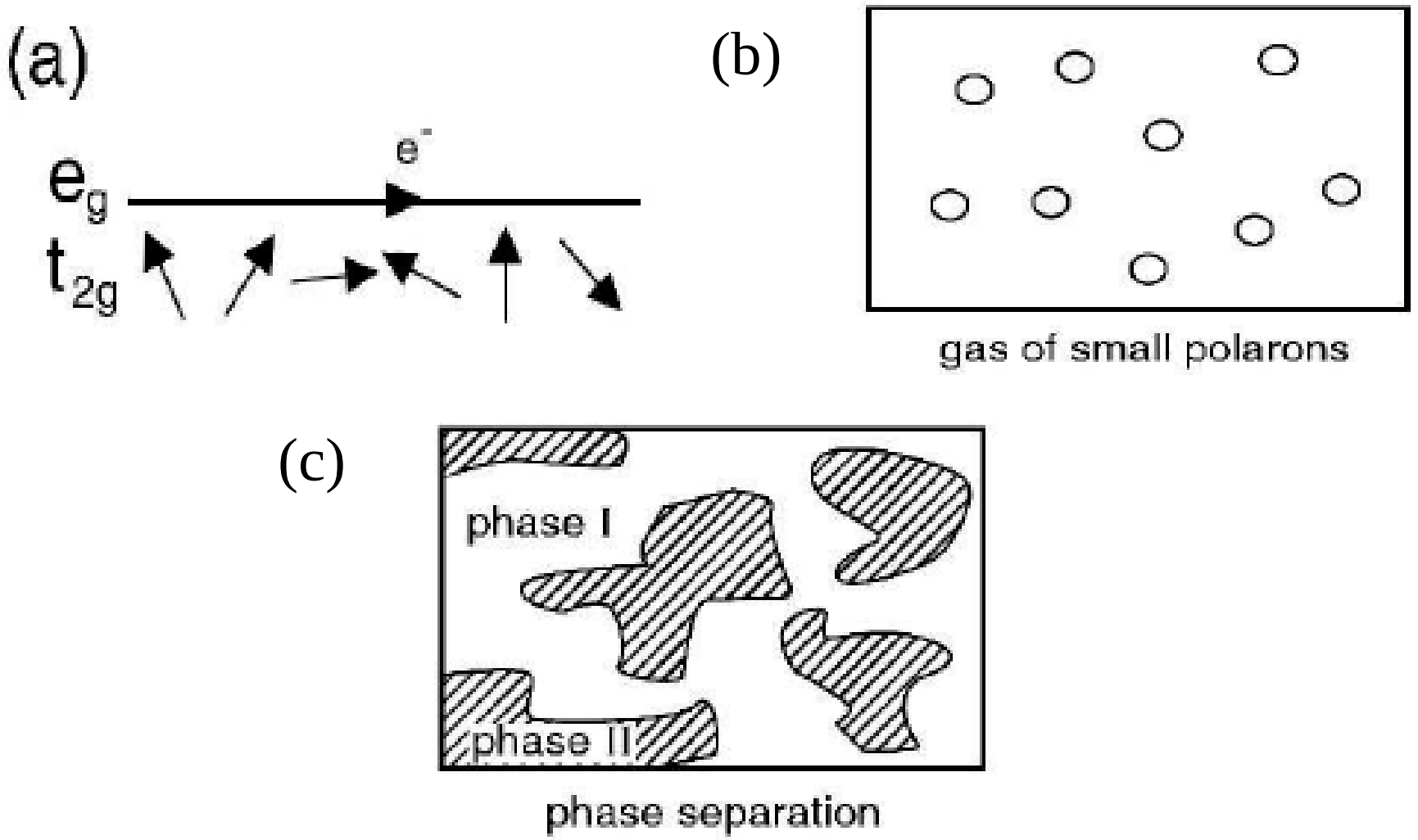

FIG. 4. Schematic representation of theories for manganites. (a) is a simple “double exchange” scenario, without phase competition. (b) is based on a gas of polarons above the Curie temperature T_C, also without phase competition. In (c), a phase-separated state above the ordering temperatures is sketched.

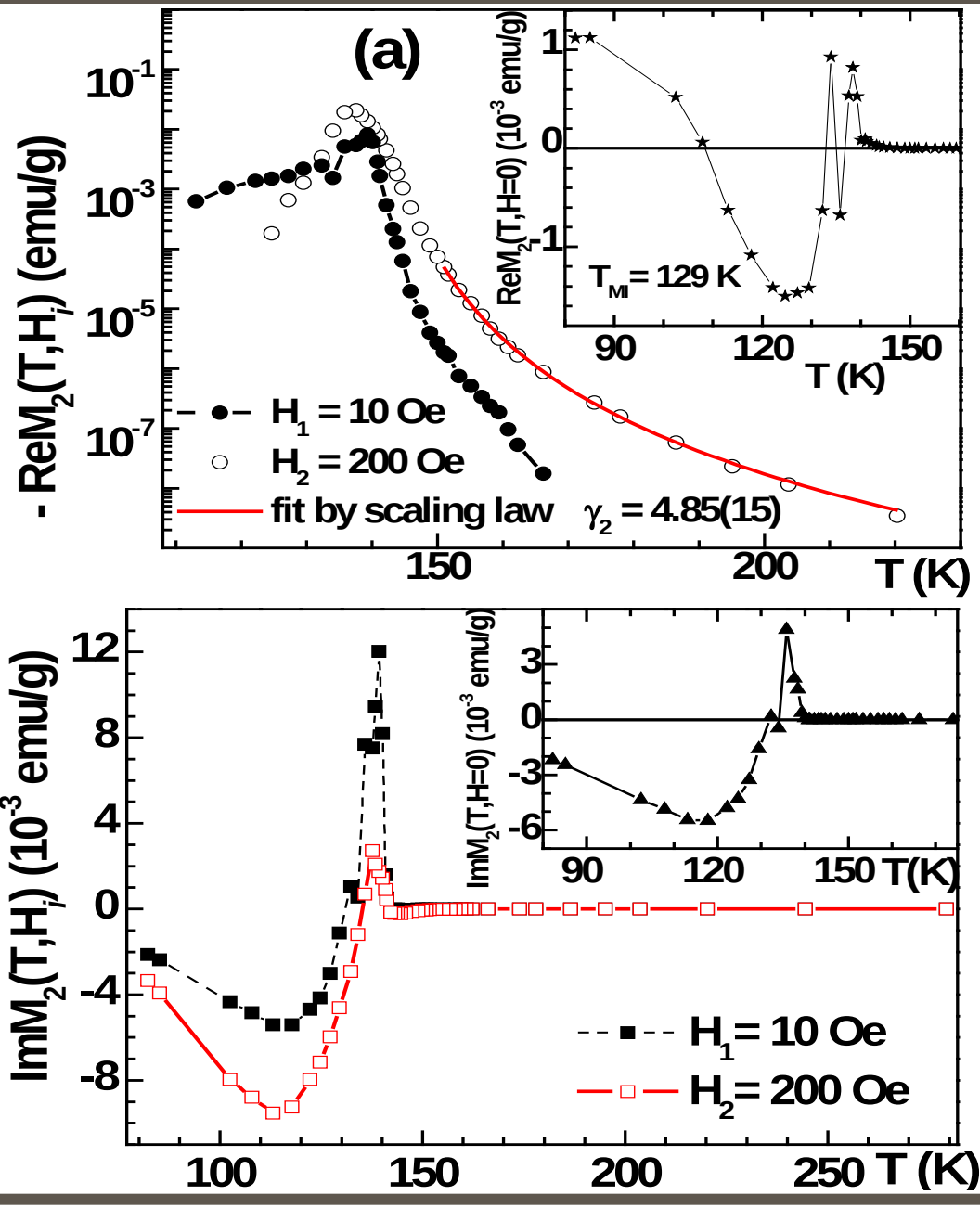

$Nd_{0.7}Ba_{0.3}MnO_3$: Re $M_2(H,T)$ и Im $M_2(H,T)$ при разных значениях H: На вставках приведены зависимости Re$M_2(H = 0, T) \propto M_{sp}$ и Im$M2(H = 0, T)$.